Supporting Information

Nanochemistry in the Gas Phase: Coulombic Adducts of Atomically Precise Noble Metal Nanoclusters and their Concomitant Reactions

Swetashree Acharya,[a] Seth Adam Horn,[b] Vikash Khokar,[c] Nicolas J. Pizzala,[b] Vivek Yadav,[a] Subrata Duary,[a] Tomas Base,*[e] De en Jiang,*[c,d] Scott A. McLuckey*[b] and Thalappil Pradeep*[a]

[a]DST Unit of Nanoscience (DSTUNS) and Thematic Unit of Excellence (TUE), Department of Chemistry, IIT Madras, Chennai, Tamil Nadu, 600036, India

[b]James Tarpo Jr. and Margaret Tarpo Department of Chemistry, Purdue University, West Lafayette, Indiana, 47906-2084, USA

[c]Interdisciplinary Materials Science, Vanderbilt University, Nashville, Tennessee 37235, USA

[d]Department of Chemical and Biomolecular Engineering, Vanderbilt University, Nashville, Tennessee 37235, USA

[e]Department of Syntheses, Institute of Inorganic Chemistry, The Czech Academy of Science, 1001 Husinec, Rez 25068, Czech Republic

Email: tbase@iic.cas.cz

Email: de-en.jiang@vanderbilt.edu

E-mail: mcluckey@purdue.edu

E-mail: pradeep@iitm.ac.in

This Supporting Information includes:

Figures S1-S18

Table of Contents

Experimental Section

Chemicals and solvents. We purchased silver nitrate ($AgNO_3$) from Rankem Chemicals. Copper(I) chloride (CuCl, 97.0%), chloroauric acid ($HAuCl_4$, 98.0%), 1,2-bis(diphenylphosphino)ethane (DPPE, 98.0%), triphenylphosphine (TPP, 98.0%), 1,4-bis(diphenylphosphino)butane (DPPB, 98.0%), 2-phenylethanethiol (2-PET) (98%), 2,4-dimethylbenzenethiol (2,4-DMBT) (≥95%), 2,5-dimethylbenzenethiol (2,5-DMBT) (≥95%), 1,3-benzenedithiol (BDT) (≥99%), tetraphenylphosphonium bromide (PPh_4Br), tetraoctyl ammonium bromide (TAOBr), palladium acetate ($Pd(OAc)_2$), chloroplatinic acid (K_2PtCl_4), sodium borohydride ($NaBH_4$, 98%), and triethylamine (Et_3N) were procured from Sigma-Aldrich. The ortho-carborane-1-thiol (o_1-CBT) was synthesized from ortho-carborane derivative, purchased from Katchem, Czech Republic. Crystalline o_1-CBT ligands were used for the NC synthesis. The meta-carborane-9-thiol (m_9-CBT) ligands were purchased from Katchem s.r.o. (Czech Republic). MCT ligand was re-crystallized from hot chloroform/hexane solvents for NC synthesis. All HPLC grade solvents, tetrahydrofuran (THF), dichloromethane (DCM), methanol (MeOH), dimethylformamide (DMF), and acetonitrile (ACN) were purchased from Rankem Chemicals and Finar, India. All compounds were used without additional purification.

Synthesis of $[Ag_{17}(o_1\text{-CBT})_{12}]^{3-}$. The Ag_{17} NC was synthesised using the method used in our previous report[1] with a slightly altered version of the Brust method that was reported earlier.[2] After dissolving around 38 mg of $AgNO_3$ in 2 mL of MeOH, roughly 17 mL of DCM was added. After adding about 90 μL of DMBT to this solution, a thick yellow mixture was produced. Approximately 6 mg of PPh_4Br in 0.5 mL of MeOH was added after 5 minutes, followed by the addition of 15 mg $NaBH_4$ in 0.5 mL ice-cold water, after 20 minutes into the reaction mixture. The reaction mixture was stirred for approximately 8 hours and then aged for 24 hours. The reaction produced a dark brown solution that was centrifuged. The supernatant was collected in a round-bottom flask and concentrated using a rotary evaporator to a volume of 2 millilitres. After that, the NC was precipitated by adding excess MeOH and then repeatedly cleaned with MeOH. Finally, the NCs were extracted by dissolving the precipitate in DCM.

Synthesis of $[Ag_{13}Cu_4(o_1\text{-CBT})_{12}]^{3-}$. To synthesize this bimetallic NC $Ag_{13}Cu_4$, a similar synthetic procedure as that of the above-mentioned Ag_{17} was employed.[1] For the $Ag_{13}Cu_4$, a starting reagent consisting of 20 mg $AgNO_3$ and 20 mg of CuCl was used. Following a reaction time of 18 h, the resulting $Ag_{13}Cu_4$ NC exhibited an orange-brown color solution in DCM. The

cluster was purified by thoroughly washing with MeOH/H_2O followed by complete solvent evaporation with final extraction in DCM.

Synthesis of $[Cu_{14}(o_{9,12}\text{-CBDT})_6]^+$. The Cu_{14} NC was synthesised using the method used in our previous report.[3] First the $[Cu_{18}(DPPE)_6H_{16}]^{2+}$ NC was synthesized using a modified synthetic protocol from the literature.[4] In brief, 95 mg (0.49 mM) of CuI was mixed with 120 mg (0.03 mM) of DPPE under argon and then 15 ml of acetonitrile (as received) was added to it. After 30 min of additional stirring, the as-formed white complexes were reduced by directly adding 180–185 mg of dry $NaBH_4$ powder. After another hour of stirring at room temperature, an orange-colored precipitate was formed, which indicated the formation of the crude product. The final product was collected as an orange solid by centrifugation and further washed three times using 5 ml of acetonitrile and methanol each in succession, to remove excess starting reagents. Finally, the solid product, Cu_{18}, was dissolved in DCM and used for further reactions.

Synthesis of $[Ag_{21}(m_9\text{-CBT})_{12}(TPP)_2]^+$. The Ag_{21} NC was prepared using the method used in our previous report using the LEIST reaction of $[Ag_{18}(TPP)_{10}H_{16}]^{2+}$ NC[5] with MCT ligands.[6] In brief, 8 mg of MCT ligands are added to a solution having 10 mg of Ag18 nanocluster in 5 ml methanol. After 10 min of the addition of thiol, the solution became yellowish and which eventually converted to dark red. After 2 hours of reaction, a dark reddish solution forms as an end product. After overnight size focusing, centrifugation of the reaction mixture ends up a reddish precipitate, which was extracted in DCM after the multiple cleaning of methanol. As prepared Ag_{21} nanoclusters are insoluble in methanol but soluble in DCM, chloroform and DMF. Suitable quality single crystals are grown following the vapor diffusion of hexane into a concentrated cluster solution in DCM. The yield of the product is 65% in terms of Ag_{18} nanocluster. The formed Ag_{21} nanocluster with twelve MCT and two TPP ligands is the predominant product during this LEIST reaction.

Synthesis of $[Ag_{22}(DPPB)_4(2,5\text{-DMBT})_{12}Cl_4]^{2+}$. The Ag_{22} NC was synthesised using our previous report[7] modifying the reported method. In a typical one-pot synthesis, ~20 mg of $AgNO_3$ was dissolved in MeOH/DCM (5/9 v/v) followed by the addition of 10 μL of 2,5-DMBT. Then 10 mg of DPPB was added to the reaction mixture and kept stirring. After 15−20 min, 20 mg of $NaBH_4$ (in 1 mL of ice-cold water) was added dropwise to the mixture, which changed the color from yellow to dark brown. After that, 10 mg of PPh_4Cl and 30 μL of triethylamine were added. The reaction was kept under stirring for 12 h under ice-cold conditions. After completion of the reaction, it was kept for 2−3 days at 4 °C. The mixture was

then thoroughly washed with MeOH/H_2O followed by complete solvent evaporation. Then the NC was extracted using MeOH and dried on a rotavapor. All measurements were performed in MeOH.

Synthesis of $[Au_{25}(PET)_{18}]^-$. For the synthesis of Au_{25} NC, we followed a previously published protocol.[8] About 40 mg of $HAuCl_4.3H_2O$ was taken in 7.5 ml THF and mixed with 65 mg of TAOBr and stirred for around 15 min to get an orange-red solution. To the solution, PET was added in 1:5 molar ratio (68 µL) and stirred for another hour. This resulted in Au-thiolate formation. The as-formed thiolate was then reduced by adding about 39 mg of $NaBH_4$ in ice-cold water. The color changed from yellow to brown. The solution was allowed to stir for another 5 hours for complete conversion and size focusing synthesis of $[Au_{25}(PET)_{18}]^-$. The as synthesized cluster was then vacuum dried by rotavapor and precipitated using excess MeOH to get rid of free thiol and excess thiolate. The process was repeated a few times. Then the Au_{25} NC was extracted into acetone and centrifuged, and the supernatant solution was collected leaving behind a precipitate consisting of larger clusters. The acetone solution was vacuum dried. Finally, the cluster was dissolved in dichloromethane (DCM) and centrifuged and the supernatant solution was collected which consisted of the pure cluster.

Synthesis of $[MAg_{24}(DMBT)_{18}]^{2-}$ (M= Pd, Pt). For the synthesis of $PdAg_{24}$ and $PdAg_{24}$, we adhered to a previously published protocol.[9] First, approximately 10 mg of $AgNO_3$ and approximately 10 mg of $Pd(OAc)_2$ or K_2PtCl_4 were dissolved in 5 mL of MeOH along with 9 mL of DCM, respectively. Subsequently, around 10 µL of DMBT in 0.5 mL of DCM was added to the reaction mixture followed by approximately 10 mg of PPh_4Br in 0.5 mL of DCM addition. The NCs were formed when 40 mg $NaBH_4$ in 0.5 mL ice-cold water was introduced to the reaction mixture after 20 minutes, followed by addition of 50 µL of triethylamine after 5 min interval with overnight stirring. The formed NC solution was evaporated, and the residue was washed with MeOH. The NCs were extracted with DCM.

Synthesis of $[Ag_{29}(BDT)_{12}(PPh_3)_4]^{3-}$. The NC was synthesized by adopting an already reported method.[10] First, around 20 mg of $AgNO_3$ was dissolved in 5 mL of MeOH, and then 9 mL of DCM was added. After a few minutes, approximately 13.5 µL of BDT in 0.5 mL of DCM was added to the solution. Then, after 5 min of stirring in the dark, nearly 200 mg of PPh_3 in 0.5 mL of DCM was added to the mixture, and next, 0.5 mL of an ice-cold aqueous solution of 11 mg $NaBH_4$ was added, which immediately changed the color of the solution to dark brown. The reaction was kept for 3 h under dark conditions. Then, the red precipitate was

collected by centrifugation. The NC was washed several times with MeOH and the residue was dissolved in DMF. The reddish orange NCs were collected after the removal of unwanted byproducts.

Instrumentation

Mass Spectrometry. All experiments were conducted on a modified SCIEX TripleTOF 5600 (MDS SCIEX, Concord, Ontario, Canada). Modifications include the ability to apply: quadrupolar DC to the rodset of the collision cell (q2), alternating current waveforms to the lenses on either side of the collision cell, and external waveforms for dipolar resonant excitation in q2, among others.[11] For these reactions, ions were generated via nESI and sequentially introduced into the instrument. Separate nESI sources were utilized to prevent solution phase reactions, as detailed previously. The first ion introduced was generally larger than *m/z* 3100, due to the need of further isolation steps (resonant ejection of undesirable ions) in the collision cell of the instrument. For ions with m/z less than 3100, direct mass isolation can be performed in Q1. After the isolation of the initial analyte ion, the reagent was introduced into q2 for 600 ms of mutual storage, after which the ion of opposite polarity was discarded by switching to DC barriers at the ends of the trap. The resulting products of the ion-ion reaction could then be isolated and probed via ion trap collision induced dissociation (IT-CID).

Computational details

Density functional theory (DFT) calculations were done using the CP2K program.[12] We optimized both the NCs, and then different orientations of both the NCs were optimized to get the adduct structure, and the binding energies of the NCs were calculated for each orientation. The plane-wave cutoff of 500 Ry was used for the Gaussian Plane Wave (GPW) mixed basis-set method.[13] For atoms H, C, and S, DZVP-MOLOPT-GTH (Double-Zeta Valence Polarize (DZVP) molecular optimized (MOLOPT) Goedecker, Teter, and Hutter (GTH)) basis sets[14] were used, and for B, Cu, and Ag atoms, the DZVP-MOLOPT-SR-GTH (SR denotes shorter range) basis set was used with GTH-PBE potentials.[15] Grimme's DFT-D3 van der Waals dispersion corrections were used,[16] with Fermi-Dirac smearing and Broyden charge mixing. The PBE exchange-correlation functional by Perdew-Burke-Ernzerhof[17] was used with an SCF

convergence of 10^{-5}. For atom relaxation for geometry optimization, the force convergence was 4.5 x 10-4 Hartree/Bohr with the BFGS method.

The binding energy of the adduct with different orientations of NCs was calculated with the following equation-

$$BE = E\{[Ag_{17}(o_1\text{-}CBT)_{12}]^{3-}\} + E\{[Cu_{14}(o_{9,12}\text{-}CBDT)_6]^{+}\} - E\{[Ag_{17}(o_1\text{-}CBT)_{12}Cu_{14}(o_{9,12}\text{-}CBDT)_6]^{2-}\}$$

The atom exchange reaction energy was calculated with the following equation-

$$\Delta E = E\{[Ag_{17-n}Cu_n(o_1\text{-}CBT)_{12}Cu_{14-n}Cu_n(o_{9,12}\text{-}CBDT)_6]^{2-}\} - E\{[Ag_{17}(o_1\text{-}CBT)_{12}Cu_{14}(o_{9,12}\text{-}CBDT)_6]^{2-}\}$$

Where n is the number of metal atoms exchanged in the adduct.

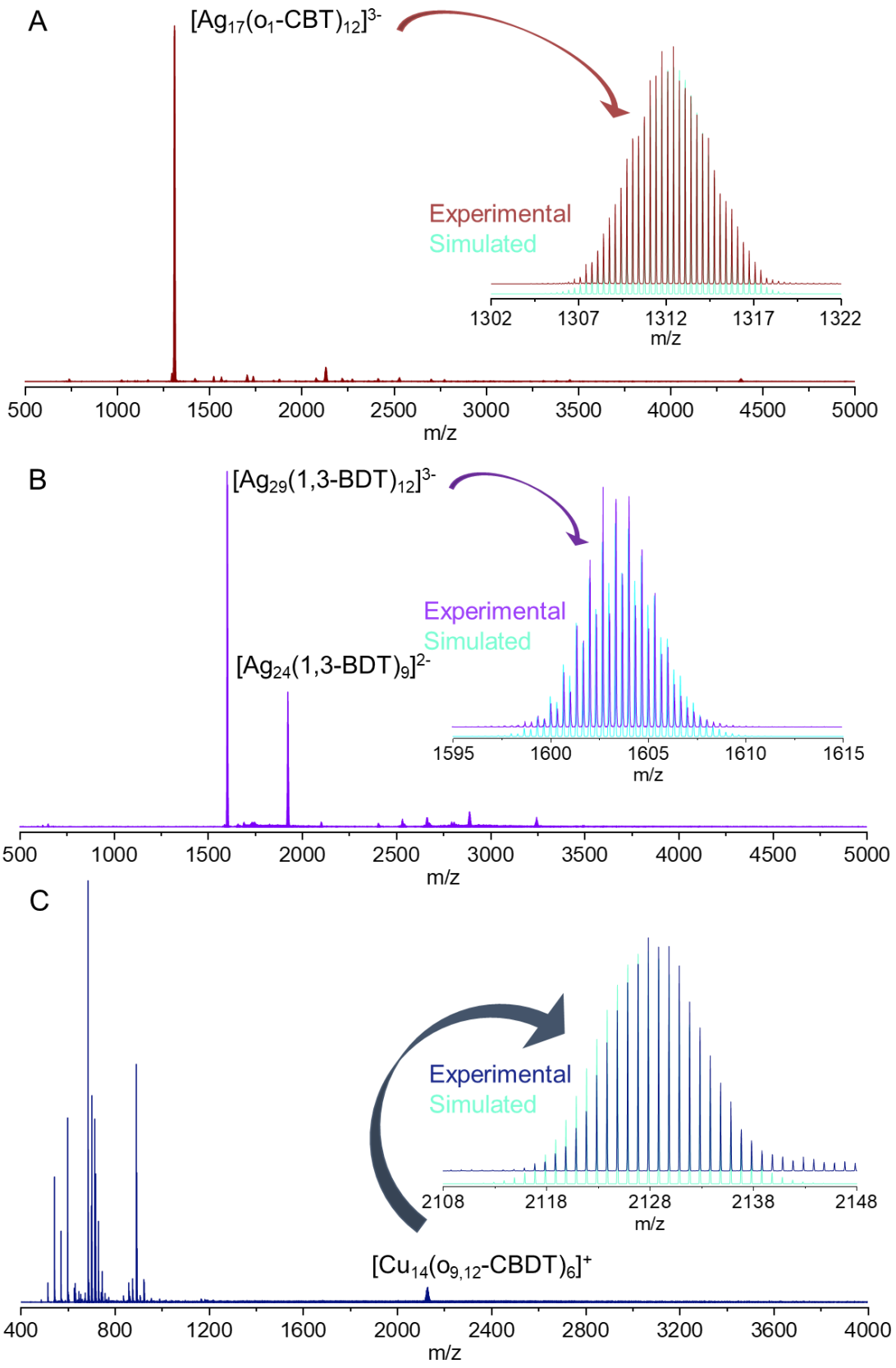

Figure S1. nESI MS of the (A) $[Ag_{17}(o_1\text{-CBT})_{12}]^{3-}$, (B) $[Ag_{29}(1,3\text{-BDT})_{12}]^{3-}$ and (C) $[Cu_{14}(o_{9,12}\text{-CBDT})_6]^{+}$ NCs. Inset shows the comparison of the isotopic distribution of the simulated and experimental peak for each NC ions.

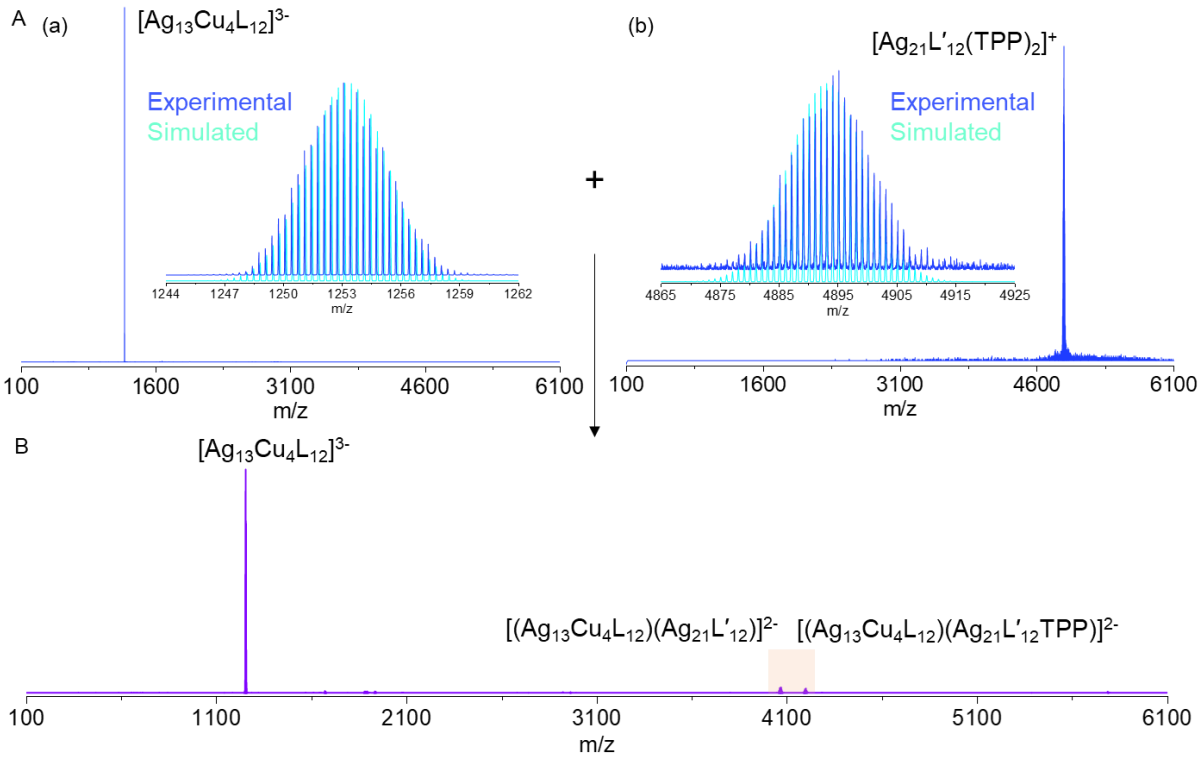

Figure S2. Mass spectrum of isolated (A(a)) $[Ag_{13}Cu_4L_{12}]^{2-}$ and (A(b)) $[Ag_{21}L'_{12}(TPP)_2]^{+}$, where the inset shows the comparison of the isotopic distribution of the simulated and experimental peak for each NC ions. (B) The reaction products were formed through Coulombic interaction between the two NC ions. Here L = o_1-CBT, L′ = m_9-CBT.

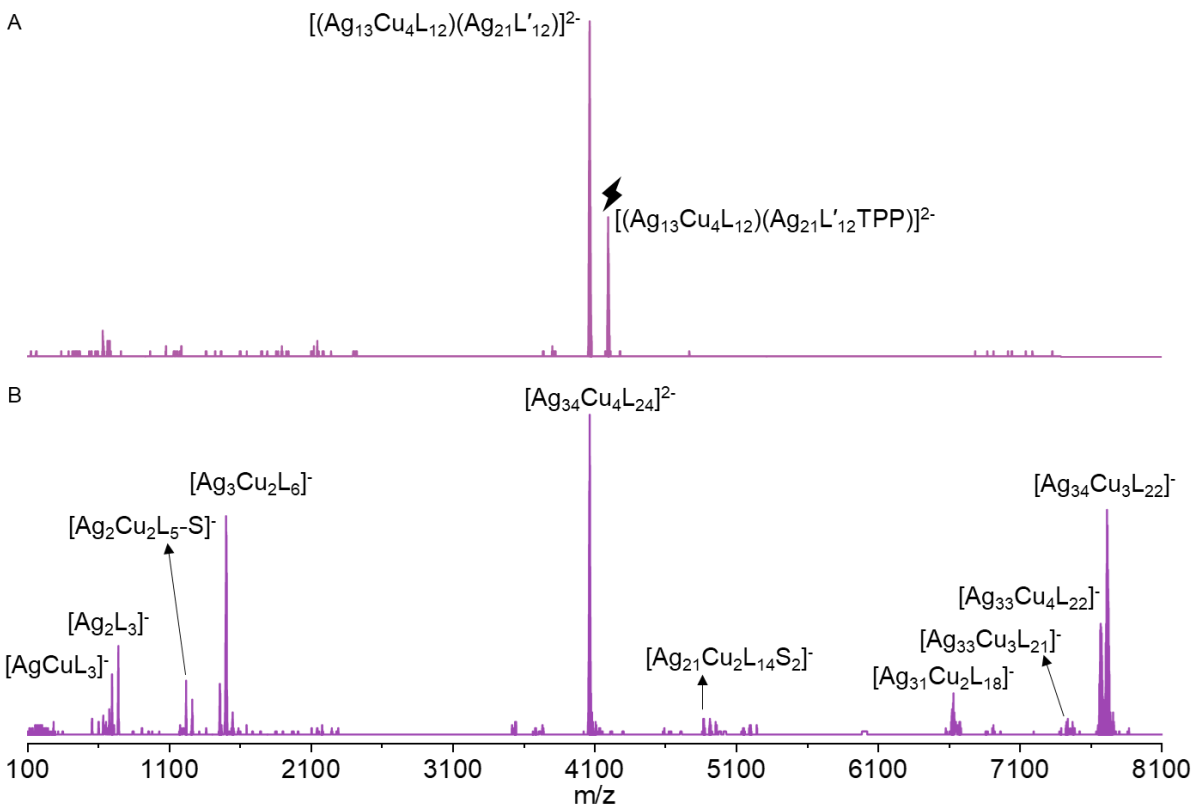

Figure S3. Mass spectrum of isolated adducts (A) $[Ag_{13}Cu_4L_{12}Ag_{21}L'_{12}]^{2-}$ and $[Ag_{13}Cu_4L_{12}Ag_{21}L'_{12}TPP]^{2-}$ formed during Coulombic interaction of $[Ag_{13}Cu_4L_{12}]^{3-}$ and $[Ag_{21}L'_{12}]^{+}$. (B) MS/MS of $[Ag_{13}Cu_4L_{12}Ag_{21}L'_{12}TPP]^{2-}$ using ITCID showing different species generated during fragmentation. Here L = o_1-CBT, L′ = m_9-CBT. (Note that the mass of L and L′ in these two NCs is equal and cannot be distinguished during fragmentation.)

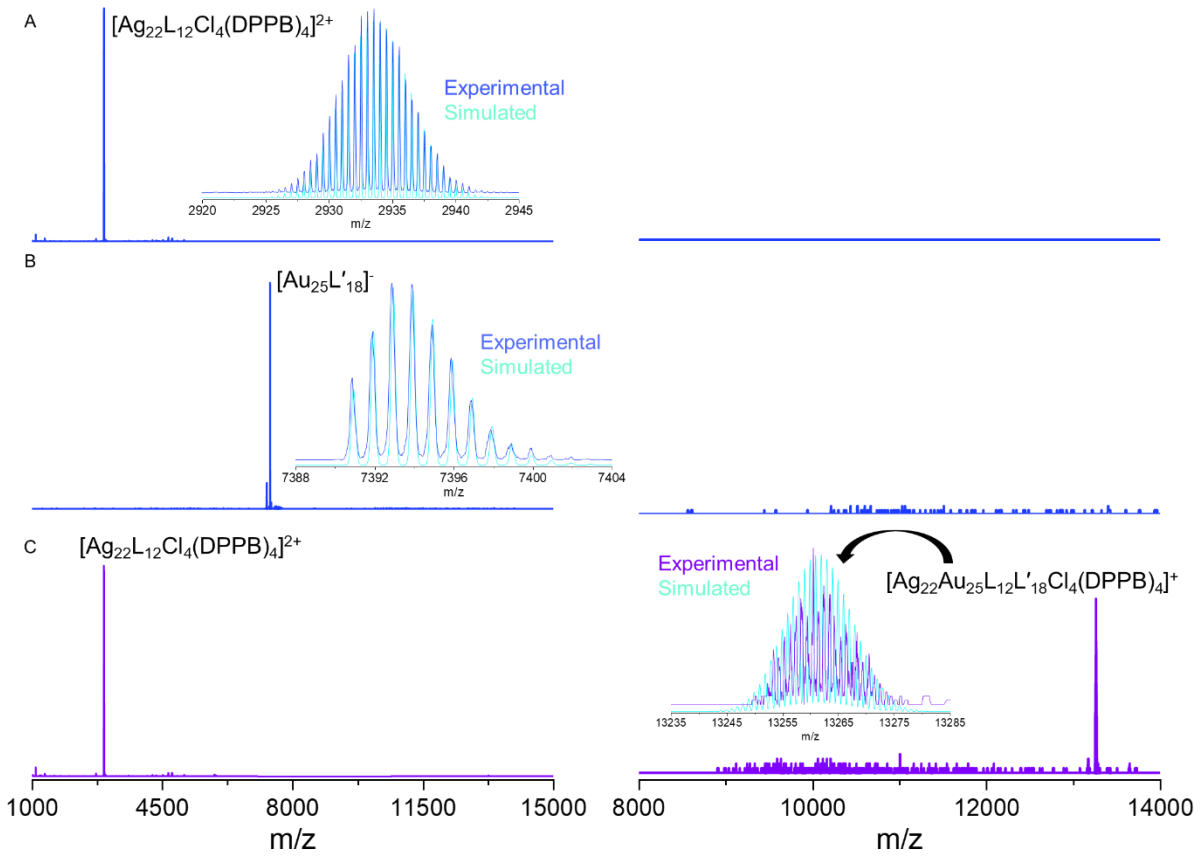

Figure S4. Mass spectrum of isolated (A) $[Ag_{22}L_{12}Cl_4(DPPB)_4]^{2+}$, (B) $[Au_{25}L'_{18}]^-$ and (C) reaction products formed through Coulombic interaction between the two NC ions. The right side shows the expanded high mass region for the isolated adduct $[Ag_{22}L_{12}Cl_4(DPPB)_4Au_{25}L'_{18}]^+$. Insets show the comparison of simulated and experimental isotopic distribution. Here L = 2,5-DMBT, L′ = PET.

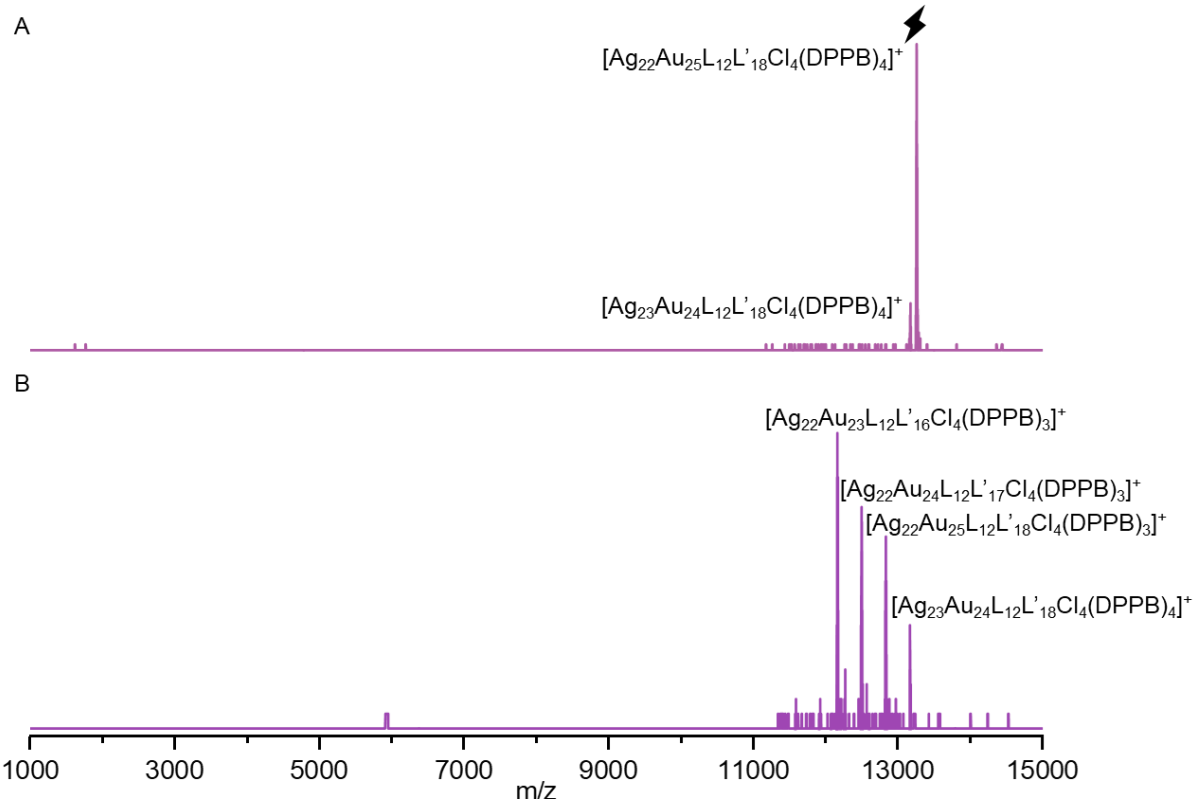

Figure S5. (A) Mass spectrum of isolated adduct $[Ag_{22}L_{12}Cl_4(DPPB)_4Au_{25}L'_{18}]^+$. (B) MS/MS of $[Ag_{22}L_{12}Cl_4(DPPB)_4Au_{25}L'_{18}]^+$ using ITCID showing different species generated during fragmentation. Here L = 2,5-DMBT, L′ = PET.

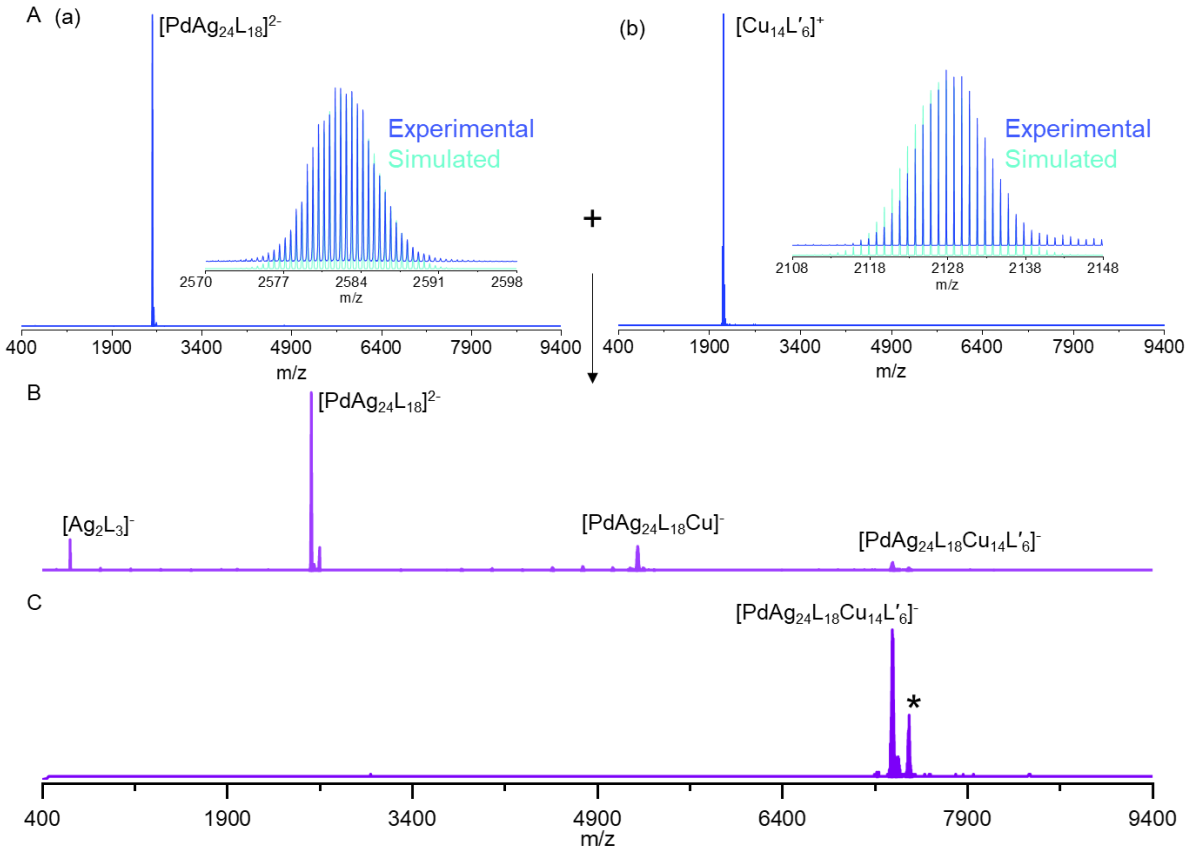

Figure S6. Mass spectrum of isolated (A(a)) $[PdAg_{24}L_{18}]^{2-}$ and (A(b)) $[Cu_{14}L'_6]^{+}$ and its insets show the comparison of simulated and experimental isotopic distribution. (B) The reaction products were formed through Coulombic interaction between the two NC ions. (C) Mass spectrum of the isolated adduct $[PtAg_{24}L_{18}Cu_{14}L'_6]^{-}$. Here L = DMBT, L′ = $o_{9,12}$-CBDT. * = $[PdAg_{24}L_{19}Cu_{14}L'_6]^{-}$.

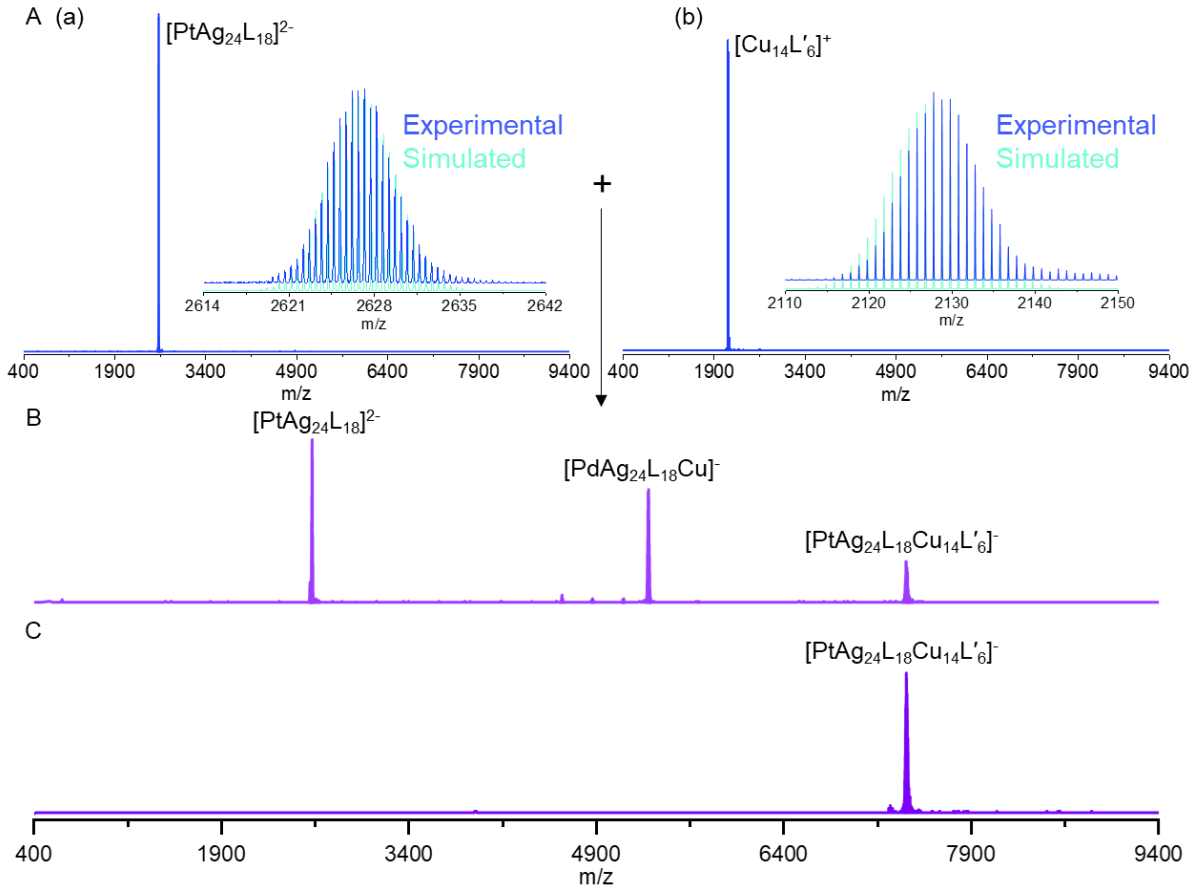

Figure S7. Mass spectrum of isolated (A(a)) $[PtAg_{24}L_{18}]^{2-}$ and (A(b)) $[Cu_{14}L'_6]^{+}$, and its insets show the comparison of simulated and experimental isotopic distribution. (B) The reaction products were formed through Coulombic interaction between the two NC ions. (C) Mass spectrum of the isolated adduct $[PtAg_{24}L_{18}Cu_{14}L'_6]^{-}$. Here L = DMBT, L′ = $o_{9,12}$-CBDT.

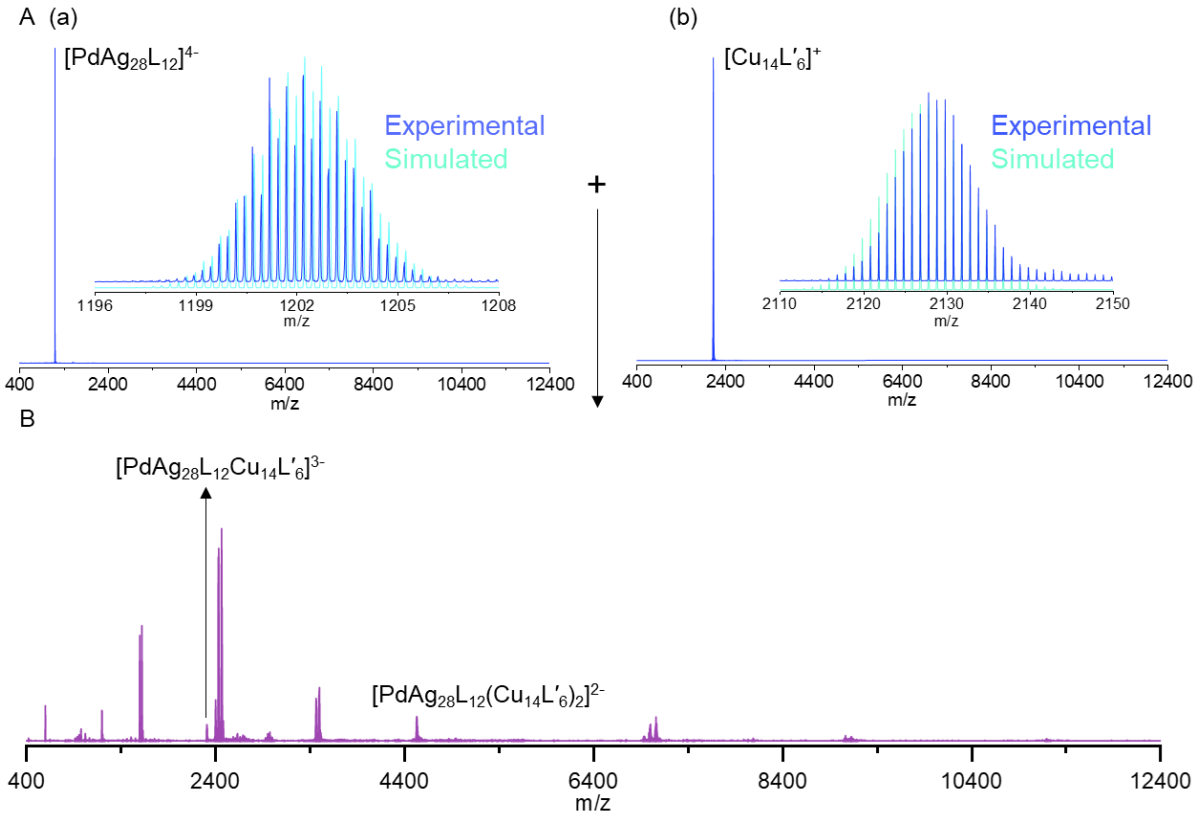

Figure S8. Mass spectrum of isolated (A(a)) $[PdAg_{28}L_{12}]^{4-}$ and (A(b)) $[Cu_{14}L'_6]^{+}$, and its insets show the comparison of simulated and experimental isotopic distribution. (B) The reaction products were formed through Coulombic interaction between the two NC ions. Here L = BDT, L′ = $o_{9,12}$-CBDT.

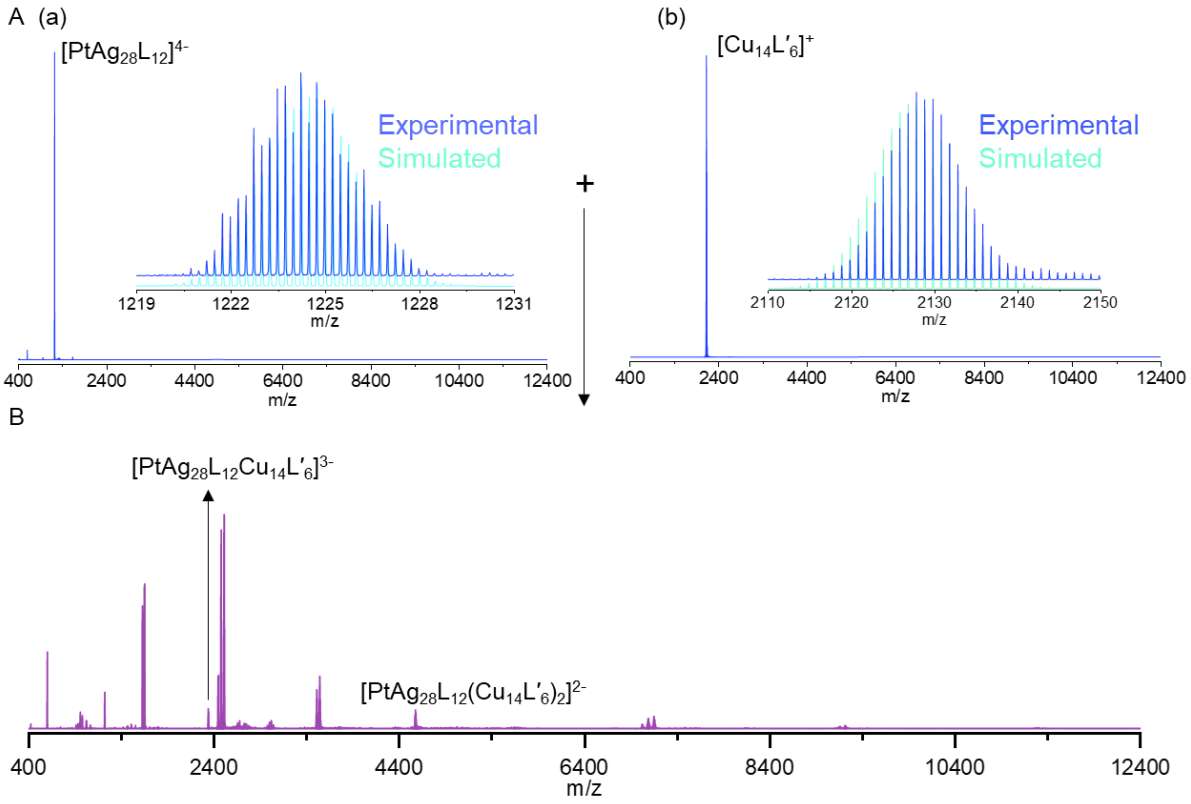

Figure S9. Mass spectrum of isolated (A(a)) $[PtAg_{28}L_{12}]^{4-}$ and (A(b)) $[Cu_{14}L'_6]^{+}$, and its insets show the comparison of simulated and experimental isotopic distribution. (B) The reaction products were formed through Coulombic interaction between the two NC ions. Here L = BDT, L′ = $o_{9,12}$-CBDT.

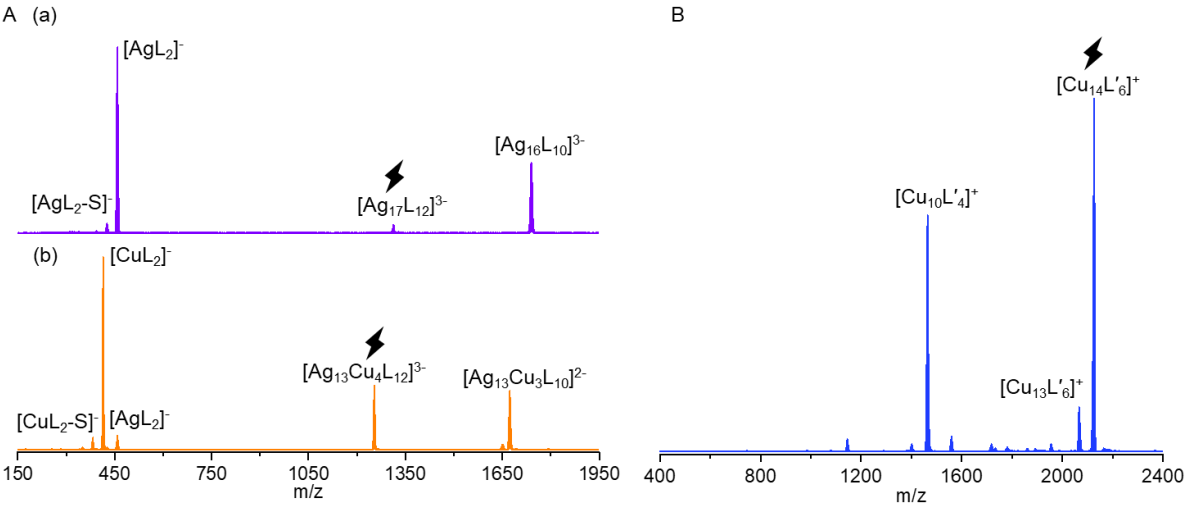

Figure S10. MS/MS spectrum of (A(a)) $[Ag_{17}L_{12}]^{3-}$, (A(b)) $[Ag_{13}Cu_4L_{12}]^{3-}$ and (B) $[Cu_{14}L'_6]^{+}$ using ITCID showing their usual fragmentation pattern.

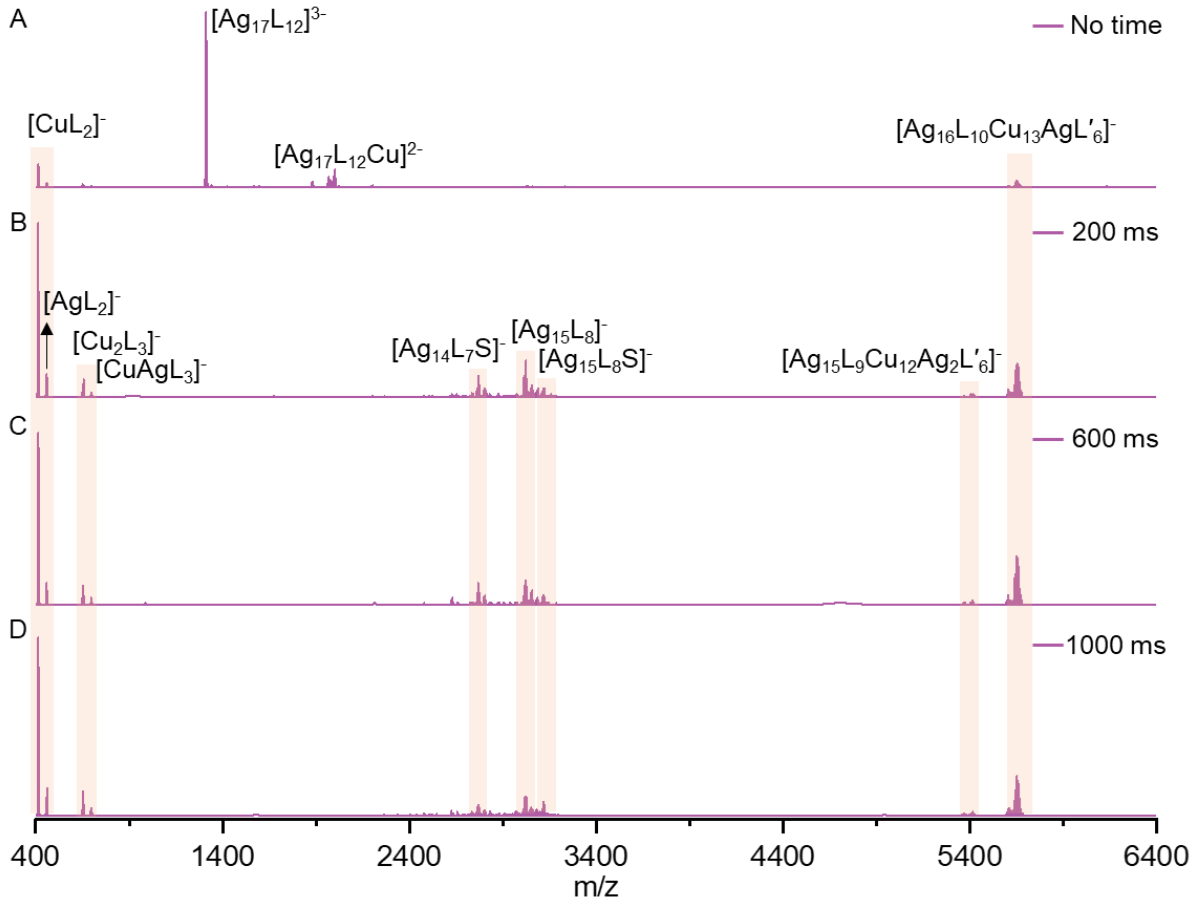

Figure S11. MS/MS spectrum of $[Ag_{17}L_{12}Cu_{14}L'_6]^{2-}$ at 40 mV collision energy using ITCID, at different trapping times i.e. (A) no time (ion activated as the reaction proceeds, such that the ion is immediately fragmented upon formation), (B) 200 ms, (C) 600 ms, and (D) 1000 ms, indicating no such difference in fragmentation pattern, confirming a faster equilibrium between the NC ions of the adduct.

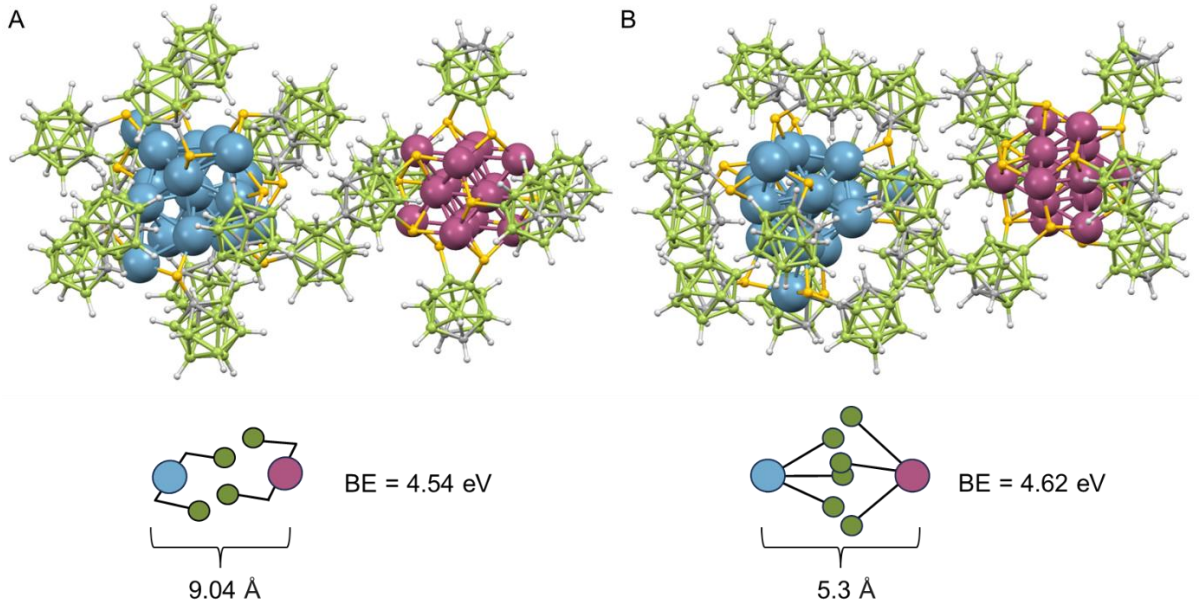

Figure S12. Two most stable arrangements of NC ions for adduct formation in the gas phase with different orientations are shown in A and B. (A) A two-on-two ligand interdigitation orientation from both the NCs, having a metal-to-metal distance of 9.04 Å having a binding energy of 4.54 eV. (B) A three-on-three ligand interdigitation orientation from both the NCs, having a metal-to-metal distance of 5.3 Å having a binding energy of 4.62 eV.

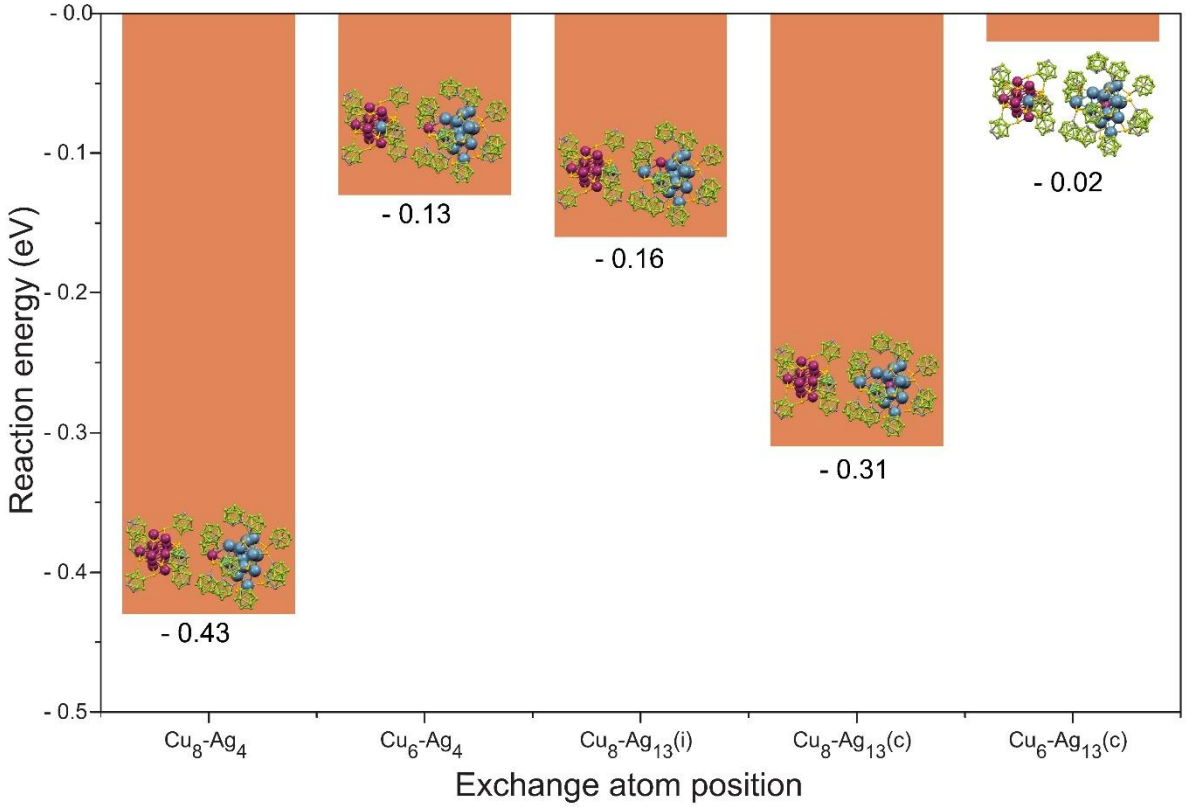

Figure S13. DFT calculated atom exchange reaction energies showing the feasibility of Cu-Ag atom exchange between distinct positions on NCs in the adduct from Cu_{14} NC to Ag_{17} NC.

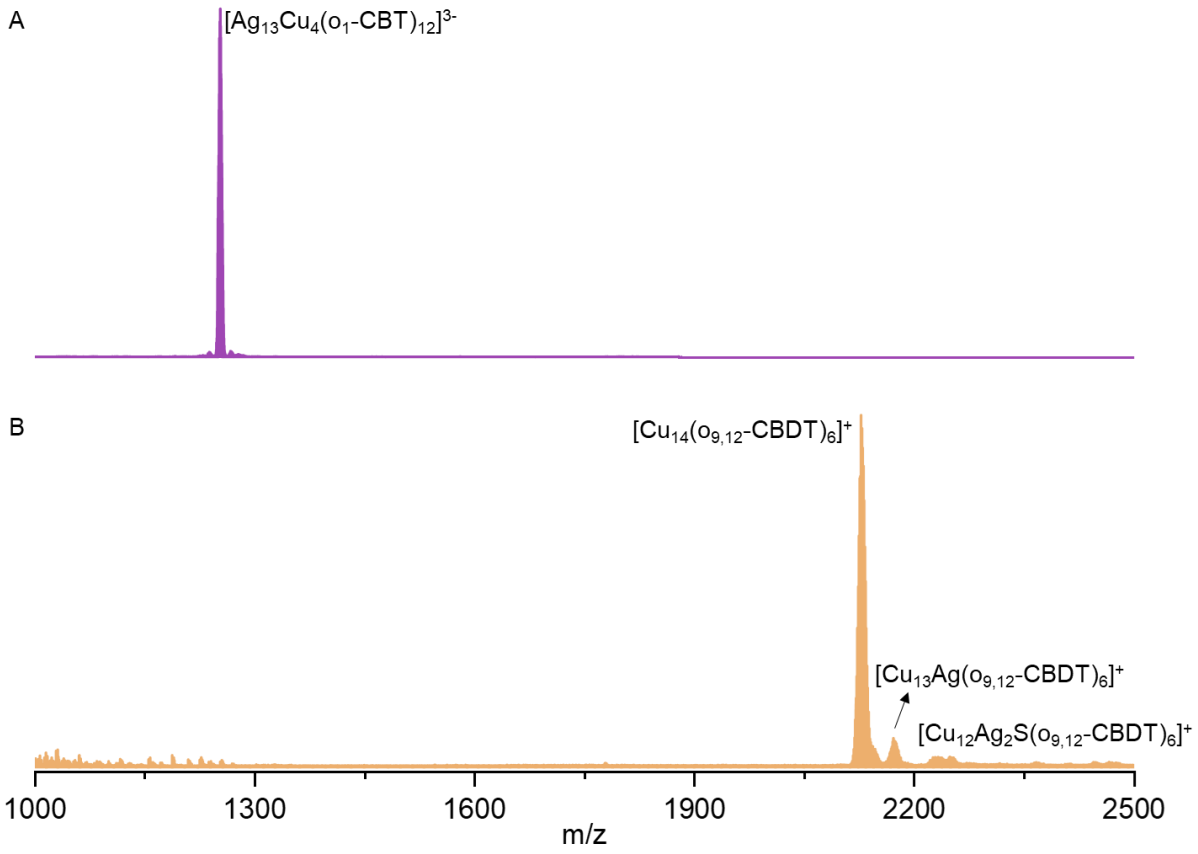

Figure S14. nESI MS of the reaction between $[Ag_{17}(o_1\text{-CBT})_{12}]^{3-}$ and $[Cu_{14}(o_{9,12}\text{-CBDT})_6]^{+}$ NCs in solution showing (A) immediate exchange of 4 Cu atoms on $[Ag_{17}(o_1\text{-CBT})_{12}]^{3-}$ NC and (B) a minimal exchange of 1-2 Ag atoms on $[Cu_{14}(o_{9,12}\text{-CBDT})_6]^{+}$ NC.

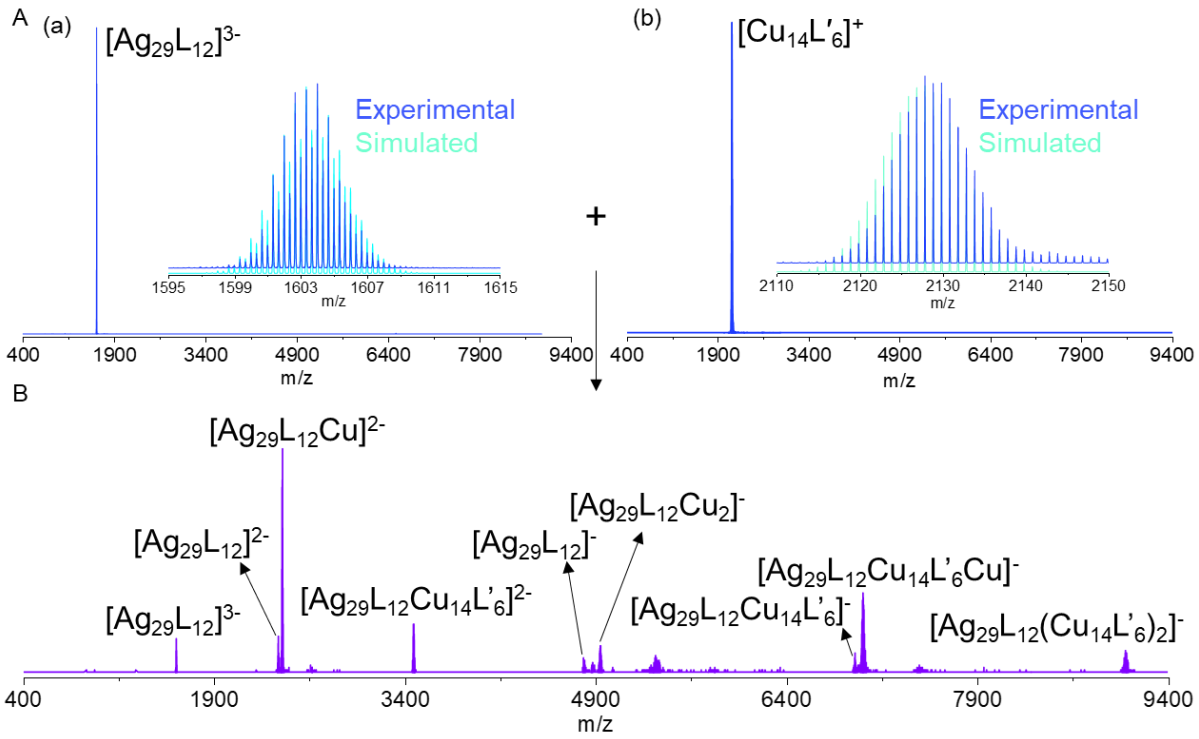

Figure S15. Mass spectrum of isolated (A(a)) $[Ag_{29}L_{12}]^{3-}$ and (A(b)) $[Cu_{14}L'_6]^{+}$ with insets showing the comparison of simulated and experimental isotopic distribution. (B) The reaction products were formed through Coulombic interaction between the two NC ions. Here L = 1,3-BDT, L′ = $o_{9,12}$-CBDT.

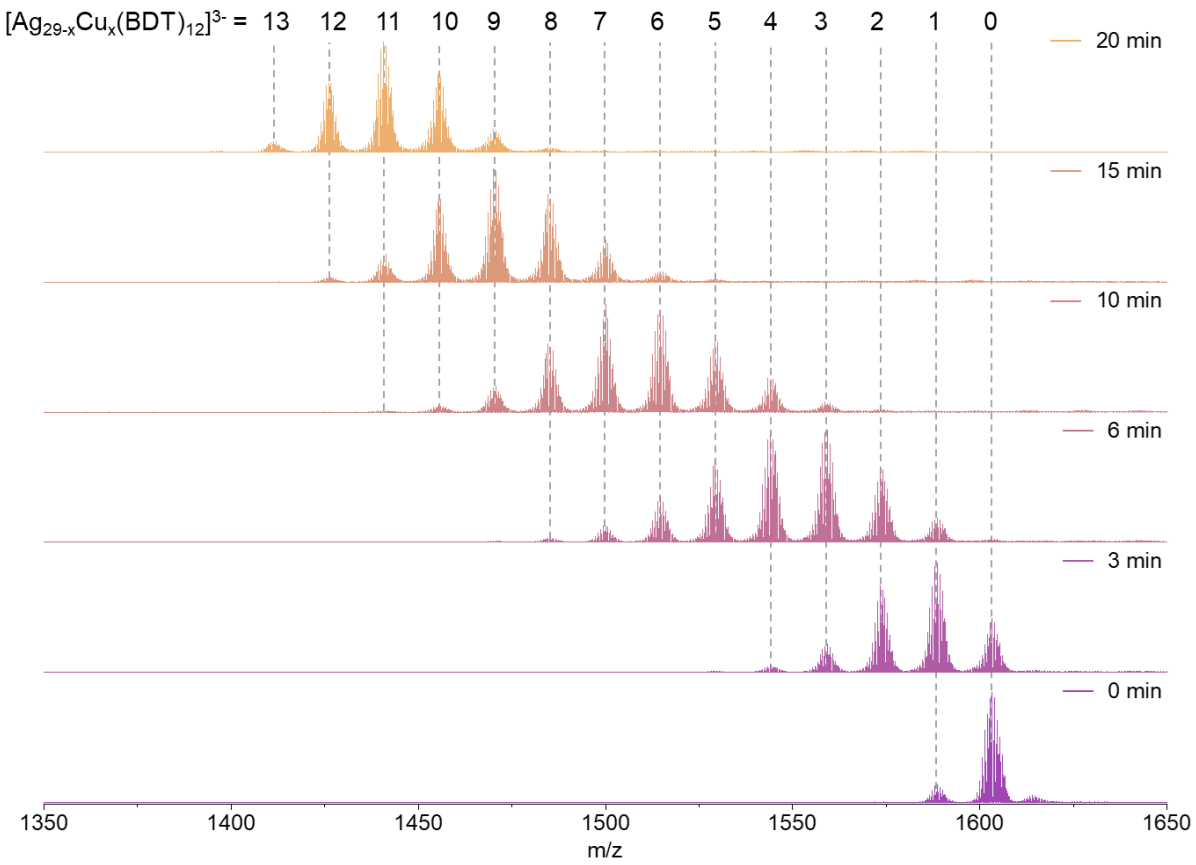

Figure S16. nESI MS of the reaction between $[Ag_{29}(BDT)_{12}]^{3-}$ and $[Cu_{14}(o_{9,12}\text{-}CBDT)_6]^{+}$ NCs in solution and the evolution of Cu doped Ag_{29} NC product species with time. Solution phase reaction between these two NCs shows up to 13 Cu-Ag exchange on the Ag_{29} NC within 20 minutes of the reaction.

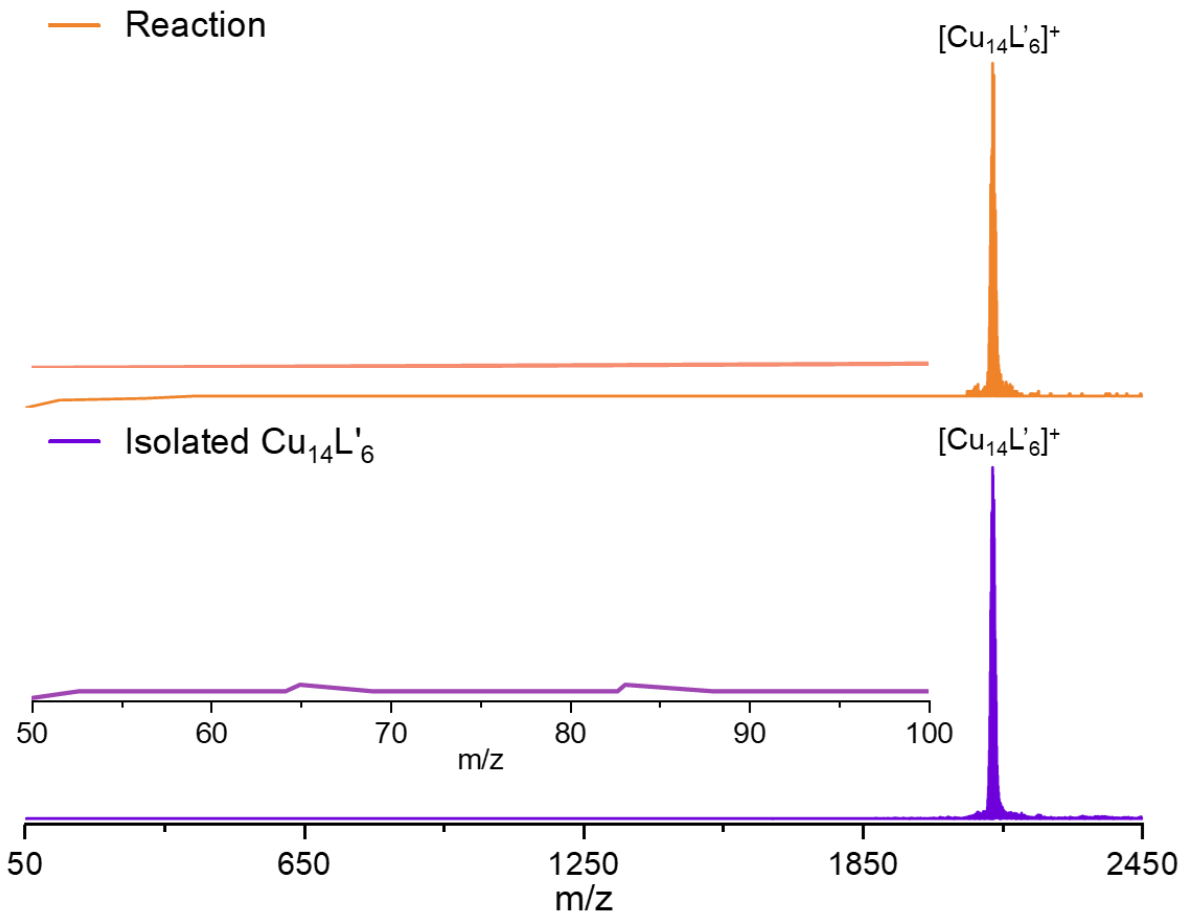

Figure S17. Positive mode mass spectrum of isolated $[Cu_{14}L'_6]^+$ at bottom panel and during the reaction between the two NC ions at the top panel is shown. Inset shows the m/z region from 50-100, confirming absence of Cu^+ species before and after coulombic interaction between the two NCs. Here, L′ = $o_{9,12}$-CBDT.

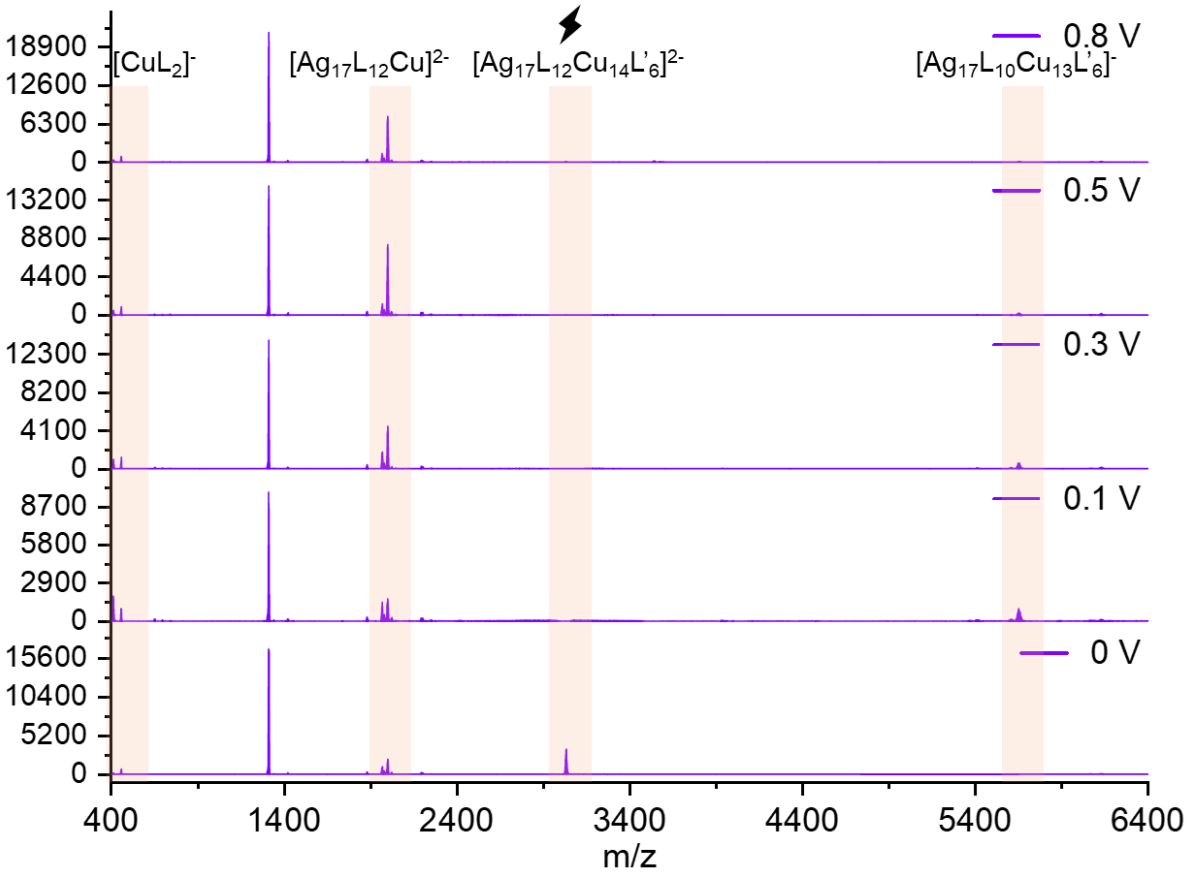

Figure S18. MS/MS spectrum of $[Ag_{17}L_{12}Cu_{14}L'_6]^{2-}$ at 40 mV collision energy using ITCID, with different oscillation voltage i.e. 0 V, 0.1 V, 0.3 V, 0.5 V, and 0.8 V, for knocking out the adduct species $[Ag_{17}L_{12}Cu_{14}L'_6]^{2-}$ without fragmenting it, indicating an increase in intensity of the $[Ag_{17}L_{12}Cu]^{2-}$ species. Here L = o_1-CBT, L′ = $o_{9,12}$-CBDT.

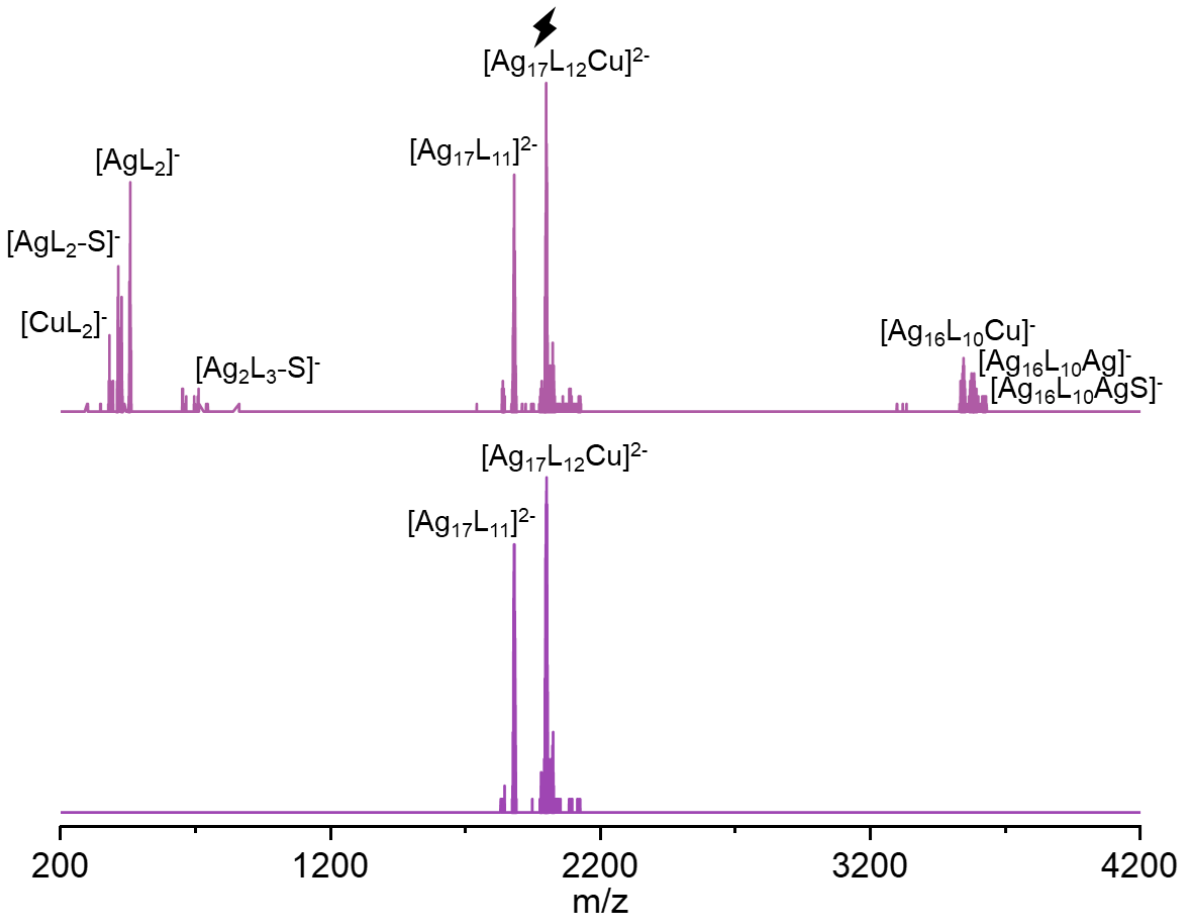

Figure S19. Bottom panel shows the mass spectrum of isolated adduct $[Ag_{17}L_{12}Cu]^{2-}$ along with $[Ag_{17}L_{11}]^{2-}$. Top panel shows the MS/MS of $[Ag_{17}L_{12}Cu]^{2-}$ using ITCID showing different species generated during fragmentation. Here L = o_1-CBT.

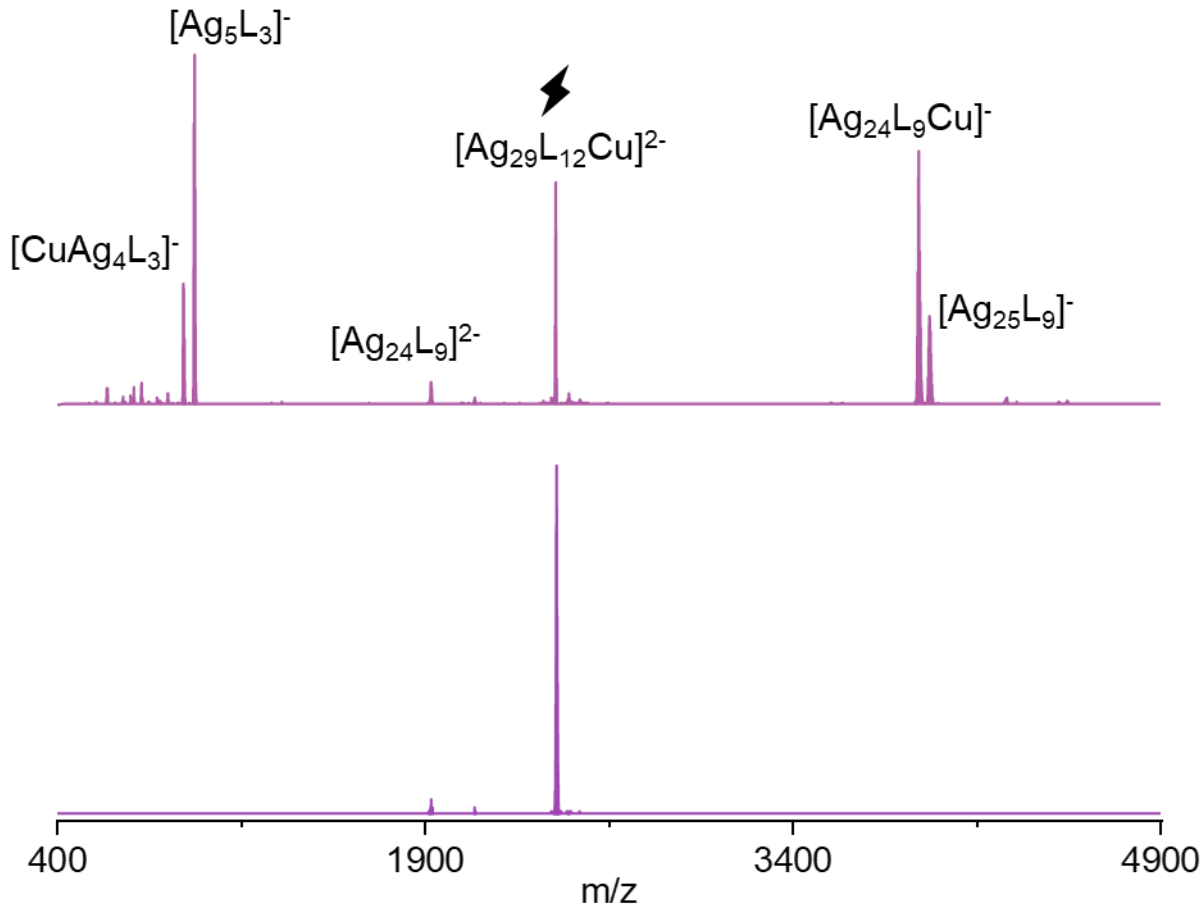

Figure S20. Bottom panel shows the mass spectrum of isolated adduct $[Ag_{29}L_{12}Cu]^{2-}$. Top panel shows the MS/MS of $[Ag_{29}L_{12}Cu]^{2-}$ using ITCID showing different species generated during fragmentation. Here L = 1,3-BDT.

References:

(1) Yadav, V.; Jana, A.; Acharya, S.; Malola, S.; Nagar, H.; Sharma, A.; Kini, A. R.; Antharjanam, S.; Machacek, J.; Adarsh, K. N. V. D.; Base, T.; Häkkinen, H.; Pradeep, T. Site-Specific Substitution in Atomically Precise Carboranethiol-Protected Nanoclusters and Concomitant Changes in Electronic Properties. *Nat. Commun.* **2025**, *16* (1), 1197. https://doi.org/10.1038/s41467-025-56385-w.

(2) Joshi, C. P.; Bootharaju, M. S.; Alhilaly, M. J.; Bakr, O. M. $[Ag_{25}(SR)_{18}]^-$: The "Golden" Silver Nanoparticle. *J. Am. Chem. Soc.* **2015**, *137* (36), 11578–11581. https://doi.org/10.1021/jacs.5b07088.

(3) Jana, A.; Duary, S.; Das, A.; Kini, A. R.; Acharya, S.; Machacek, J.; Pathak, B.; Base, T.; Pradeep, T. Multicolor Photoluminescence of Cu14 Clusters Modulated Using Surface Ligands. *Chem. Sci.* **2024**, *15* (34), 13741–13752. https://doi.org/10.1039/D4SC01566E.

(4) Li, J.; Ma, H. Z.; Reid, G. E.; Edwards, A. J.; Hong, Y.; White, J. M.; Mulder, R. J.; O'Hair, R. A. J. Synthesis and X-Ray Crystallographic Characterisation of Frustum-Shaped Ligated [Cu18H16(DPPE)6]2+ and [Cu16H14(DPPA)6]2+ Nanoclusters and Studies on Their H2 Evolution Reactions. *Chem. – Eur. J.* **2018**, *24* (9), 2070–2074. https://doi.org/10.1002/chem.201705448.

(5) Ghosh, A.; Bodiuzzaman, M.; Nag, A.; Jash, M.; Baksi, A.; Pradeep, T. Sequential Dihydrogen Desorption from Hydride-Protected Atomically Precise Silver Clusters and the Formation of Naked Clusters in the Gas Phase. *ACS Nano* **2017**, *11* (11), 11145–11151. https://doi.org/10.1021/acsnano.7b05406.

(6) Jana, A.; Unnikrishnan, P. M.; Poonia, A. K.; Roy, J.; Jash, M.; Paramasivam, G.; Machacek, J.; Adarsh, K. N. V. D.; Base, T.; Pradeep, T. Carboranethiol-Protected Propeller-Shaped Photoresponsive Silver Nanomolecule. *Inorg. Chem.* **2022**, *61* (23), 8593–8603. https://doi.org/10.1021/acs.inorgchem.2c00186.

(7) Khatun, E.; Bodiuzzaman, M.; Sugi, K. S.; Chakraborty, P.; Paramasivam, G.; Dar, W. A.; Ahuja, T.; Antharjanam, S.; Pradeep, T. Confining an Ag10 Core in an Ag12 Shell: A Four-Electron Superatom with Enhanced Photoluminescence upon Crystallization. *ACS Nano* **2019**, *13* (5), 5753–5759. https://doi.org/10.1021/acsnano.9b01189.

(8) Kang, X.; Chong, H.; Zhu, M. Au25(SR)18: The Captain of the Great Nanocluster Ship. *Nanoscale* **2018**, *10* (23), 10758–10834. https://doi.org/10.1039/C8NR02973C.

(9) Yan, J.; Su, H.; Yang, H.; Malola, S.; Lin, S.; Häkkinen, H.; Zheng, N. Total Structure and Electronic Structure Analysis of Doped Thiolated Silver [MAg24(SR)18]2– (M = Pd, Pt)

Clusters. *J. Am. Chem. Soc.* **2015**, *137* (37), 11880–11883. https://doi.org/10.1021/jacs.5b07186.

(10) AbdulHalim, L. G.; Bootharaju, M. S.; Tang, Q.; Del Gobbo, S.; AbdulHalim, R. G.; Eddaoudi, M.; Jiang, D.; Bakr, O. M. $Ag_{29}(BDT)_{12}(TPP)_4$: A Tetravalent Nanocluster. *J. Am. Chem. Soc.* **2015**, *137* (37), 11970–11975. https://doi.org/10.1021/jacs.5b04547.

(11) Bhanot, J. S.; Fabijanczuk, K. C.; Abdillahi, A. M.; Chao, H.-C.; Pizzala, N. J.; Londry, F. A.; Dziekonski, E. T.; Hager, J. W.; McLuckey, S. A. Adaptation and Operation of a Quadrupole/Time-of-Flight Tandem Mass Spectrometer for High Mass Ion/Ion Reaction Studies. *Int. J. Mass Spectrom.* **2022**, *478*, 116874. https://doi.org/10.1016/j.ijms.2022.116874.

(12) Kühne, T. D.; Iannuzzi, M.; Del Ben, M.; Rybkin, V. V.; Seewald, P.; Stein, F.; Laino, T.; Khaliullin, R. Z.; Schütt, O.; Schiffmann, F. CP2K: An Electronic Structure and Molecular Dynamics Software Package-Quickstep: Efficient and Accurate Electronic Structure Calculations. *J. Chem. Phys.* **2020**, *152* (19), 194103.

(13) VandeVondele, J.; Krack, M.; Mohamed, F.; Parrinello, M.; Chassaing, T.; Hutter, J. Quickstep: Fast and Accurate Density Functional Calculations Using a Mixed Gaussian and Plane Waves Approach. *Comput. Phys. Commun.* **2005**, *167* (2), 103–128. https://doi.org/10.1016/j.cpc.2004.12.014.

(14) VandeVondele, J.; Hutter, J. Gaussian Basis Sets for Accurate Calculations on Molecular Systems in Gas and Condensed Phases. *J. Chem. Phys.* **2007**, *127* (11), 114105. https://doi.org/10.1063/1.2770708.

(15) Perdew, J. P. Generalized Gradient Approximation Made Simple. *Phys. Rev. Lett.* **1996**, *77* (18), 3865–3868. https://doi.org/10.1103/PhysRevLett.77.3865.

(16) Grimme, S.; Antony, J.; Ehrlich, S.; Krieg, H. A Consistent and Accurate Ab Initio Parametrization of Density Functional Dispersion Correction (DFT-D) for the 94 Elements H-Pu. *J. Chem. Phys.* **2010**, *132* (15), 154104. https://doi.org/10.1063/1.3382344.

(17) Hammer, B.; Hansen, L. B.; Nørskov, J. K. Improved Adsorption Energetics within Density-Functional Theory Using Revised Perdew-Burke-Ernzerhof Functionals. *Phys. Rev. B* **1999**, *59* (11), 7413–7421. https://doi.org/10.1103/PhysRevB.59.7413.